Water Resources Research

RESEARCH ARTICLE
10.1029/2023WR036588

Effects of Leafy Flexible Vegetation on Bed-Load Transport and Dune Geometry

G. Artini[1], S. Francalanci[1], L. Solari[1], and J. Aberle[2]

[1]Department of Civil and Environmental Engineering, University of Florence, Firenze, Italy, [2]Leichtweiß-Institute for Hydraulic Engineering and Water Resources, Technische Universität Braunschweig, Braunschweig, Germany

Key Points:

- Near-bed leaves decrease the average dune wavelength and influence their tridimensionality, challenging common bedform stability diagrams
- Classical bed-load transport models proved effective in scenarios with limited frontal vegetation area and in the absence of foliage
- The presence of leafy vegetation leads to higher bed-load transport than predicted by classical sediment transport models

Supporting Information:

Supporting Information may be found in the online version of this article.

Correspondence to:

G. Artini,
giada.artini@unifi.it

Citation:

Artini, G., Francalanci, S., Solari, L., & Aberle, J. (2024). Effects of leafy flexible vegetation on bed-load transport and dune geometry. *Water Resources Research*, *60*, e2023WR036588. https://doi.org/10.1029/2023WR036588

Received 14 NOV 2023
Accepted 23 AUG 2024

Abstract The development of sustainable river management strategies requires knowledge of the effect of vegetation on hydrodynamics and sediment transport. To date, the complex physical processes involving the combined effects of leafy flexible vegetation and mobile bedforms are not completely understood. Most sediment transport models have been developed for bare bed conditions so that their performance in the presence of leafy flexible vegetation remains unclear. On the other hand, recently developed models consider vegetated conditions but they typically account only for the presence of rigid cylinders and in some cases scour at their base. For this purpose, laboratory experiments were conducted with mobile dune bed conditions and artificial flexible plants with varying Leaf Area Index to investigate the effect of flexible vegetation on bed morphology and sediment transport. Sediment transport rates and bedform characteristics such as height, wavelength and celerity, were measured in specifically designed experimental runs. The collected data show that the presence of leafy vegetation alters bed morphology, tending to reduce the average dune wavelength and leading to the formation of complex 3D geometries. Bed-shear-stress-based models for predicting sediment transport were verified to be valid under conditions of low vegetation roughness density. On the contrary, the collected data emphasize that the measured bed-load transport rate increased in the presence of leafy flexible vegetation with higher frontal area. Recent bed-load models for vegetated channels provide a better interpretation for dense leafy vegetation but are less effective when predominant effects related to dunes are present.

1. Introduction

Current river restoration strategies have a strong focus on rehabilitation by using vegetation to reduce erosion, enhance bank stability and improve habitat quality (Yager & Schmeeckle, 2013). Traditional river management strategies relied on vegetation removal to enhance channel conveyance (Box et al., 2021; Luhar & Nepf, 2013), a practice that was acknowledged as counterproductive for ecologically successful river restoration (Palmer et al., 2005).

During overbank flow, the threshold for sediment mobility is commonly exceeded in alluvial rivers, resulting in the mobilization of sediments. This mobilization may lead to the formation of bedforms, whose shape and celerity influence the sediment transport rate (Lokin et al., 2022; Naqshband et al., 2017). Additionally, floodplain vegetation commonly interacts with the flow during floods thereby impacting sediment movement (Griffin et al., 2014). Generally, plants reduce flow velocities and bed-shear stress, enhancing local deposition, thus affecting sediment transport (Nepf, 2012). Overall, natural rivers exhibit different planforms (e.g., braided and meandering patterns) shaped by sediment transport and deposition, forming floodplains and river bars that facilitate ecosystem development (Richardson et al., 2007; van Dijk, 2013). Thus, the colonization of these areas by vegetation significantly impacts the overall morphological evolution of river systems (Artini et al., 2021; Gurnell, 2014).

The current understanding of the complex physical processes governing fluvial environments remains incomplete (Wang et al., 2023). The majority of studies on vegetation-flow-sediment interaction considered mainly flat bed conditions and the effect of bedforms has mainly been overlooked (Huai et al., 2021; Le Bouteiller & Venditti, 2015; Yang & Nepf, 2019). In addition to flat bed conditions, some studies have also investigated scour holes, which generate around the stems (Armanini & Cavedon, 2019; D'Ippolito et al., 2023; Duan & Al-Asadi, 2022). For instance, Chen et al. (2012) examined the effects of submerged bundled plastic fibers and found that vegetation density directly impacts parameters like scour depth, dune height, and scour hole characteristics. Specifically, a decrease in vegetation density led to increased values of these parameters. Similarly, Follett and

Nepf (2012) conducted a laboratory study focusing on sediment patterns around emergent reedy vegetation patches in a sand bed. Their findings supported the hypothesis that dense vegetation patches cause substantial flow diversion that results in increased downstream sediment transport and deposition along the centerline of the vegetation patch. The studies conducted by Hongwu et al. (2013) and Yang et al. (2016) focused on the effects of emergent rigid vegetation in open channels. Both studies reported that the presence of vegetation reduced the incipient motion of sediment compared to bare channels, highlighting the role of vegetation in influencing sediment dynamics. Furthermore, Yager and Schmeeckle (2013) conducted experiments involving rigid cylinders and mobile sand beds. Their findings indicated that the presence of vegetation influenced the formation of non-migrating bedforms, with dimensions scaling with the distance between vegetation patches. The authors found that common models to predict sediment transport rates based on bed shear stress are inaccurate in the presence of vegetation and depositional bedforms.

Moreover, the method of Simons et al. (1965) for predicting bed-load transport rate based on the sediment mass conservation principle has been found a good approximation to predict sediment transport in channels without vegetation but not in vegetated channels where vegetation tends to decrease the migration rate or even suppresses bedforms (Nepf, 2012; Przyborowski et al., 2018; Yang & Nepf, 2019).

Additionally, recent models for predicting sediment transport have been developed considering rigid cylinders as an idealized representation of vegetation (Vargas-Luna et al., 2015). For example, the formulation proposed by Duan and Al-Asadi (2022) accounts for the solid volume fraction of the stems, while Armanini and Cavedon (2019) considered the stems mean diameter and density. However, these models are limited in their applicability to the conditions for which they were developed: leafless, rigid vegetation and absence of larger-scale bedforms, such as dunes. It is not clear whether these models can be applied to leafy flexible vegetation due to its distinct hydraulic behavior (Järvelä, 2004).

Thus, modeling vegetation in flume experiments requires progress in reproducing realistic vegetation since riparian vegetation consists of woody plants, shrubs and grasses that can not be accurately represented by rigid cylinders (Aberle & Järvelä, 2013; Box et al., 2021). Moreover, this brief review shows that a knowledge gap remains regarding the morphodynamic response of sand beds to vegetation, especially when dealing with leafy flexible vegetation. This gap is particularly critical when designing river restoration projects, as their effectiveness and success is based on the availability of reliable tools capable of predicting the morphodynamic evolution of the river system (Armanini & Cavedon, 2019; D'Ippolito et al., 2023).

The focus of this paper is on environments where young leafy and flexible vegetation colonizes regions prone to the occurrence of dunes, such as alluvial floodplains, river bars (Vargas-Luna et al., 2015), and drainage ditches (Rowiński et al., 2018). This study presents a part of the results of the PhD thesis of Artini (2023), which aimed at investigating the effects of various Leaf Area Index (LAI) values on the sediment transport, flow field and flow resistance. For this purpose, experiments were conducted under mobile bed conditions employing leafy flexible artificial vegetation with removable branches, maintaining just-submerged conditions. The same plants were utilized in previous works focusing the effects of leaf mass on the flow field and resistance. Importantly, flow velocity measurements were conducted during the experiments presented in this work, however the details of flow measurements are presented in a chapter of the PhD thesis (Artini, 2023) focused on characterizing the turbulent flow field in this complex set-up (Artini, 2023). Specifically, the aim of this work is to investigate the effects of leafy flexible vegetation on sediment transport rate and bedform characteristics, that is, geometry and celerity. Various existing models and methods for predicting sediment transport rates and bedform characteristics were evaluated for their applicability in vegetated conditions. These formulations, having originally been designed for non-vegetative scenarios, have been used as benchmarks for vegetation-free conditions. This approach provided valuable insights into the modifications of dune characteristics and the bed-load transport rate attributed to the presence of vegetation. Additionally, measured bed-load transport rates were compared with predictions made using formulation considering the presence of rigid cylinders, shedding light onto the complex interplay among flow, vegetation, sediment transport, and bedforms. The paper is structured as follows: Section 2 describes details about the experimental setup, procedure, and measurements; Section 3 presents the results; Section 4 discusses the main findings of this paper.

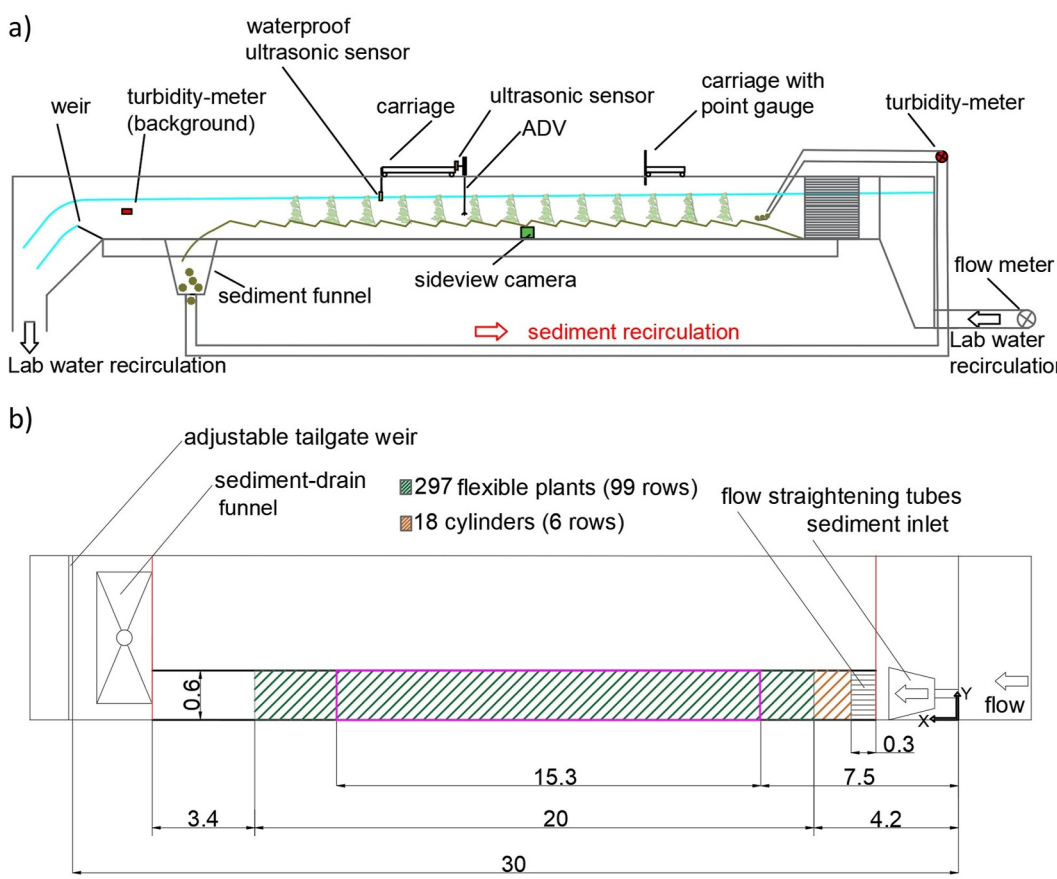

Figure 1. Schematic representation of flume setup: (a) side view; (b) plan view. Flow direction right to left. The figure is not to scale.

2. Material and Methods

2.1. Experimental Setup

Experiments were conducted in a 2 m wide, 0.8 m high, and 30 m long tiltable sediment recirculating flume in the hydraulic laboratory of the Leichtweiß-Institut for Hydraulic Engineering and Water Resources at the Technische Universität Braunschweig (Figure 1). For the experiments, the flume width was reduced to 0.6 m to recreate the same conditions as in previous experiments carried out with the same plants (described below) but under fixed-bed conditions (Schoneboom, 2011; Schoneboom & Aberle, 2009). Additionally, a PVC plate with pre-located holes was attached to the flume bottom so that the plants could be installed using 15 cm-long rigid carbon extensions (see the red rectangles in Figure 2 showing a part of these extension). At the beginning of the experimental campaign, these extensions were flushed with the screeded sediment surface of the installed 15 cm high mobile sand layer ($D_{50} = 0.84\ mm, \sigma_g = (D_{84}/D_{16})^{0.5} = 1.32$; Table S1 in Supporting Information S1). During sediment transport conditions, the sand exiting the flume was collected in a sediment trap at the downstream end of the flume, recirculated, and fed back as a water-sediment mixture at the upstream end. The flow entering the flume was conditioned by flow straightening tubes that were positioned at the flume inlet section and followed by a few rows of rigid cylinders (Figure 1).

A total of 297 artificial flexible vegetation elements were used in the experiments to ensure that the vegetation properties remained constant throughout the experimental campaign. Each plant was 23 cm high and had a three mm thick coated wire stem, four removable branches, and a blossom located at the apex of the plant. Moreover, each branch was equipped with three leaves, which were made of highly flexible dyed textile. According to Schoneboom et al. (2008), the hydrodynamic properties of the used artificial plants resemble natural black poplar twigs, a pioneer tree species that dominates the riparian areas of European rivers (Holloway et al., 2017). We note

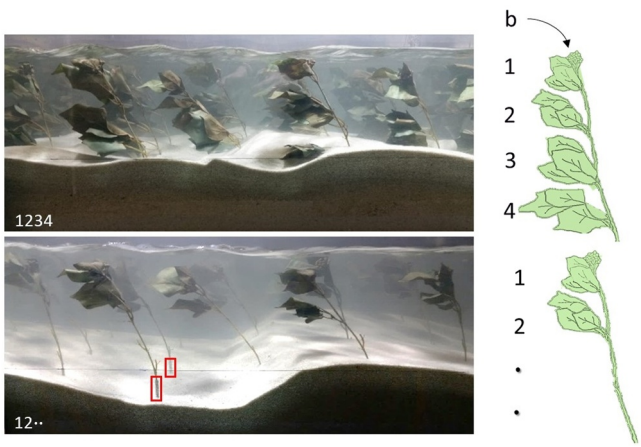

Figure 2. Frames of side-view videos taken during fully foliated (1234) setup and mid leafed (12●●) setup. Figures S9–S14 in Supporting Information S1 show side-view photos from the other experimental setups. The red rectangles highlight the rigid extension used to connect the plants to the flume bottom.

that the hydrodynamic characteristics of the artificial plants, along with the one-sided leaf area, the vegetation-to-water volume ratio and the volume of the plants were determined in previous studies (e.g., Aberle et al., 2011; Jalonen et al., 2013; Schoneboom & Aberle, 2009) and used as benchmarks for this work. In total, seven different foliage configurations were used in the experiments ranging from fully foliated to bare stem scenarios. These different configurations were obtained by removing one or more branches from the plants, so that the LAI ranged from 0.93 to 0 (Table S2 in Supporting Information S1). More details about the plants characteristics are reported in the Text S1 in Supporting Information S1. We note that a LAI lower than 1 represents conditions of low leaf mass for the plants (Box et al., 2021). However, available field measurements indicate an average LAI of 0.967 for young poplars (Antonarakis et al., 2010), which corresponds to the fully foliated setup in this study. Particularly, the vegetation setups and the hydraulic conditions considered in this study do not directly represent realistic field conditions but were chosen to match those from previous studies. The setup name, as reported in Table 1, provides information about the foliage configuration in the experimental runs. Numbers 1 to 4 indicate the attached branches, with 1 defining the top level and 4 the bottom (near-bed) branch, respectively. The letter "b" denotes the blossom, and "●" identifies the removed branch (Figure 2). The blossom was present in all plant setups, except for the ●●●● configuration. The leaves were present in all the setups except the b●●●● and ●●●● configurations.

The described plant foliage configurations were firstly employed by other studies (e.g., Aberle et al., 2011; Jalonen et al., 2013; Schoneboom, 2011; Schoneboom & Aberle, 2009), which mainly focused on the drag force exerted by the plants under various hydraulic conditions and setups, with a special focus on the effect of the leaves. An innovative addition of this work to these previous investigations that were carried out with a fixed bed, is the consideration of mobile bed conditions which led to the occurrence of dunes. The plants were arranged in a staggered pattern along the 20 m long vegetation section with a spacing of 20 cm in both directions, starting at a distance of 4.2 m from the flume inlet. The plant spacing resulted in a plant density of $m = 25$ plants/m^2 corresponding to one of the densities used by Jalonen et al. (2013), which is the only density for which the authors reported data on streamlining effects and drag force measurements for all the chosen foliage setups. An additional experimental run was conducted without vegetation (i.e., bare bed conditions) to provide a reference run with the aim to investigate the effects of the presence of vegetation on the channel conveyance at fixed bed slope and water depth. As detailed in Section 2.2, the experiments were conducted sequentially, starting with a fully foliated setup (1234) and ending with the bare bed scenario, allowing for a gradual increase in flow discharge values with each

Table 1
Experimental Conditions

Setup	Q (l/s)	H (m)	U (m/s)	Fr (−)	t_0 (h)	$S_b \pm \delta$ (RMSE) (%)	$S_E \pm \delta$ (RMSE) (%)	ΔQ (%)
1234	47.8	0.22	0.36	0.24	10.2 (56)	0.90 ± 0.0065 (0.12)	0.91 ± 0.0006 (0.01)	−63
123●	51.5	0.22	0.38	0.26	6.2 (80)	0.88 ± 0.0091 (0.16)	0.89 ± 0.0007 (0.01)	−61
12●4	53.0	0.22	0.39	0.26	11.2 (48)	0.85 ± 0.0074 (0.13)	0.86 ± 0.0008 (0.01)	−59
12●●	60.5	0.22	0.46	0.31	6.6 (56)	1.01 ± 0.0110 (0.20)	0.90 ± 0.0013 (0.02)	−54
1●●●	73.4	0.22	0.55	0.37	5.8 (64)	0.98 ± 0.0105 (0.19)	0.87 ± 0.0020 (0.04)	−44
b●●●●	94.1	0.23	0.69	0.46	3.6 (48)	0.86 ± 0.0074 (0.18)	0.84 ± 0.0032 (0.05)	−28
●●●●	106.1	0.22	0.81	0.55	*n.d.* (32)	0.76 ± 0.0097 (0.13)	0.76 ± 0.0027 (0.06)	−19
bare bed	130.5	0.22	0.97	0.65	2.8 (3)	0.48 ± 0.0079 (0.14)	0.52 ± 0.0043 (0.08)	0

Note. Water discharge Q, water depth H, channel-averaged flow velocity U and Froude number Fr of the experiments. t_0 represents the predicted durations for achieving equilibrium (Parker, 2003); the values between brackets () are the actual durations of the experimental runs. The average bed slope S_b and the energy slope S_E are reported with the ± 95% confidence intervals and the uncertainty estimated as the root mean square error (RMSE) of the linear regression. ΔQ denotes the observed reduction in channel conveyance resulting from different plant configurations compared to the bare bed setup.

run. Thus, the hydraulic conditions of this final experiment resulted closer to the upper regime, and it was decided to not pursue further investigations for this setup.

All experiments were conducted under quasi-uniform flow conditions with an average water depth of 0.22 m (Table 1) so that the deflected plants were just submerged. These conditions were selected to prevent the formation of canopy-scale vortices at the interface between the free flow and the top of the canopy. This maintained a consistent water depth for all setups, preventing the effects of turbulent eddies associated with submerged conditions. Since a fixed water depth was used for each setup, the relative submergence of the plants was assessed (Section 3) to confirm that the bending degree of the stem did not vary significantly among the experiments. In each experimental run, flow conditions were adjusted by regulating the water level using a weir located at the end of the flume and controlling the discharge through a valve. The flume slope was kept constant at $S = 0.9\%$ for all experimental runs. This slope was predetermined to ensure sediment transport in all setups by estimating the expected bed-load transport rate using the Meyer-Peter and Müller (1948) formula and using the critical Shields number according to Cao et al. (2006). Thus, since all the runs were characterized by similar water depth and slope, all experiments had comparable total shear stress, including the vegetation drag and the dunes form drag. The total shear stress was estimated using the depth-slope formulation $\tau = \rho g H S_E$, where ρ is the water density, g the gravitational acceleration, H the average water depth and S_E the energy slope.

The bed-load sediment transport rates were measured by means of two Negele turbidity-meter sensors. One sensor was placed at the flume outlet, downstream the sediment-drain funnel to measure clear water reference conditions (background value), while the other one was placed in the return pipe of the sediment recirculating system to measure the turbidity of the water-sediment mixture entering the sediment-drain funnel (labeled as sediment funnel in Figure 1a). This flux consisted of bed load from the moving dunes reaching the end of the flume. A calibration relationship was established to effectively relate the voltage difference (Δ_V) observed in the signals of the two turbidity meters to the corresponding sediment transport rate (Q_s) within an error of 3% (Equation S6 in Text S3 in Supporting Information S1). The calibration procedure consisted in two phases. The first phase aimed to associate specific bed-load transport rates with eight different outlet diameters of a sediment-filled tank positioned above the sediment-drain funnel. This involved varying the outlet diameters of the tank and measuring the corresponding bed-load transport rates Q_s by weighing the amount of sand exiting the tank within a specified time interval. The second phase aimed to correlate the known Q_s with the voltage difference between the background turbidity meter and the turbidity meter located in the sediment recirculating system. The readings of the two turbidity meters were related using an $offset$ value. At the beginning of each experimental day, the $offset$ value was determined in calm water conditions (i.e., with no discharge). Further details about the calibration procedure can be found in the Text S3 in Supporting Information S1. Since the calibration of the system was based on the voltage difference between the background turbidity meter and the turbidity meter located in the sediment recirculating system, direct measurements of the fraction of suspended sediment transport were not possible.

The water discharge Q was continuously measured during the experimental runs with a Krohne magnetic flow meter with an accuracy of $\pm$ 0.3%. The water surface was periodically scanned using a mic +130/IU/TC ultrasonic sensor with a resolution of 1 mm (accuracy $\pm$ 0.57 mm). The sensor was mounted on an automated carriage system, and scans were conducted along the centerline of the channel. A submerged Sonometer05 ultrasonic sensor with a resolution of 1 mm (accuracy of up to 1%) was used to scan the bottom topography along three longitudinal lines: $y = 15$ cm, $y = 30$ cm (middle line), and $y = 45$ cm to the left flume wall ($y = 0$ corresponds to the hydraulic left-handed side coordinate system of the flume). The bed scans were conducted immediately after the water surface scans, under clear water conditions. This was achieved by turning off the water discharge and raising the weir height at the end of the flume to suppress sediment transport while preventing the flume from draining completely. This was done only at the end of each experimental day, which lasted approximately 8 hr, to minimize interference with the ongoing experiment. The effective scanned section, highlighted as a pink rectangle in Figure 1b, spanned 15.3 m and was located between $x = 7.5$ m and $x = 22.8$ m, with $x = 0$ at the inlet section of the flume.

Flow velocity measurements were taken using a Nortek Acoustic Doppler Velocimeters at 27 vertical positions within the vegetation canopy. The velocity components were measured point-by-point at morphological equilibrium (see Section 3) with a sampling rate of 100 Hz for a duration of 3 min with a vertical spacing of 1 cm. The z-coordinates were normalized relative to the mean bed level of the specific run, which was determined through the bed elevation scans. The number of measurement points in the profiles varied depending on the local bed

topography due to the changing geometry of the bedforms along the flume. The measurement section was 7.7 m long covering between 6 and 13 dunes depending on the average wavelength associated with the specific run. The length of the measurement section was designed to allow for the application the double-averaging method (Nikora et al., 2007).

2.2. Experimental Procedure

The experimental procedure began by arranging the foliage configuration of the plants. Once the plants were set, the water flow was initiated, and the flow discharge and the height of the flume weir were adjusted to achieve just submerged conditions. Throughout each experimental run, the hydraulic conditions were maintained constant until morphological equilibrium was reached (Table 1). The morphological equilibrium was assessed by examining the correspondence between the average bed and energy slopes and by monitoring the constancy of sediment transport and dune characteristics over time, following criteria established by Simons and Richardson (1966) and Baas (1994). Upon achieving morphological equilibrium, measurements of sediment transport rate, dunes characteristic and flow velocity were collected providing a representation of the morphological equilibrium state.

Sediment lumps or waves, a phenomenon frequently encountered in recirculating flumes (Parker, 2003), were observed during the experimental runs. Therefore, the method proposed by Parker (2003) was applied to predict the time required to achieve equilibrium in each setup. The predicted durations (t_0) were significantly shorter, with a maximum of approximately 12 hr (for 12•4 setup), compared to the actual experiment durations, which ranged between 4 and 10 days (Table 1). The bare bed run was characterized by a highly turbulent flow with significant suspended sediment transport as shown in the videos taken during the experiments and provided at the repository (Artini, 2024). This run was conducted over a time period of approximately 3 hours, consistent with the predicted duration based on the Parker (2003) method. To optimize time efficiency, the experiments were conducted sequentially, with each experimental run building upon the final bed conditions of the previous run. The experimental sequence started with the fully foliated setup (1234) and concluded with the bare bed scenario, allowing for a gradual increase in flow discharge values from run to run.

At the completion of each experiment, the flume was carefully drained, and photographs of the bed topography were taken. These images were then utilized to reconstruct a digital elevation model (DEM) using the Structure-from-Motion technique (Morgan et al., 2017). The length of the section was at least 3 m long for each setup. The photos were firstly processed in Photoscan (Agisoft, 2017) to generate a point cloud, and then in Cloud Compare (Cloud compare, 2022) to remove the plants and flume walls. In areas where leaves obstructed the view, missing parts of the DEM were filled by linear interpolation using surrounding data.

2.3. Data Analysis

As mentioned before, information regarding the plant characteristics (e.g., one-sided leaf area, projected plant area) were recovered from previous works (i.e., Aberle et al., 2011; Jalonen et al., 2013; Schoneboom & Aberle, 2009), which conducted experiments with the same plants and in comparable conditions in terms of foliage, density and flow (just-submerged) conditions. The solid volume fraction ϕ was calculated as the ratio of the vegetation volume V_p to the water volume V (Lei & Nepf, 2021; Zinke, 2012). The vegetation volume (V_p) was determined using the Archimedes principle (Xu & Nepf, 2020). The resulting values were in agreement with those reported in Jalonen et al. (2013) for the relative plant setups. The roughness density was estimated as $a_z H$ for all the setups (Table 1), where $a_z = \langle a \rangle_z$ is the depth-averaged frontal area per unit volume of the plants canopy, which is defined as $\langle a \rangle_z = mA_f / h_p$, where A_f is the cumulative frontal area and h_p is the deflected plant height.

The frontal area was determined using an image analysis procedure, conducted in air, as described in Xu and Nepf (2020). For this analysis, two plants were selected and photographed against a white background from five different angles. The original plant images were transformed into black and white images, and the number of black pixels was counted at each vertical coordinate. By using a reference scale, the pixel count was converted into length obtaining the frontal area distribution $A(z)$. All the resulting $A(z)$ profiles are reported in Figures S15–S20 in Supporting Information S1. The cumulative frontal area for each foliage configuration was calculated by integrating $A(z)$ over the plant height h_p. Additionally, the value obtained from integrating $A(z)$ within the first 5 cm near the mean bed level was used to estimate the near-bed frontal area per unit volume $\langle a \rangle_{z,nb}$. Particularly,

the streamlined frontal area values, effectively related to the experimental conditions, were indirectly estimated by referencing the corresponding channel-averaged velocity U, determined using the continuity equation $U = Q/(WH)$ (where $W = 0.6$ m is the flume width), to the $A_f - U$ values reported for the relative setups in Jalonen et al. (2013). Thus, the obtained $A(z)$ from the image analysis procedure were scaled based on the reduction between the cumulative frontal area from the image analysis and the value obtained from the graph by Jalonen et al. (2013). Further details regarding plants characteristics are provided in the Text S1 in Supporting Information S1.

The bed and water surface scans were subjected to post-processing, including de-spiking and gap-filling tools in Matlab environment (R2019b). These post-processed scans were then utilized to estimate the bed and energy slopes. The energy line was estimated as $E(x) = WSE(x) + U^2(x)/(2g)$, where $U(x)$ represents the local averaged flow velocity, and $WSE(x)$ is the local water surface elevation measured through the scans. To calculate the local $U(x)$, the local water depth $H(x)$ was approximated as the difference between the water surface elevation and the bed elevation at the given x-coordinate. In fact, it is assumed that dune migration is negligible during the sediment discharge shut-off procedure carried out prior to bed scans. Recalling that the scans of WSE and bed elevation were not performed simultaneously but consecutively, the error in estimating the local water depth through these measures was considered acceptable. This is because the presence of vegetation suppressed the traditional out-of-phase behavior between the bed elevation profile and the water surface of a flow over dunes, as evident in the videos taken during the experiments and provided at the repository (Artini, 2024). Thus, the water surface was characterized by surface waves resulting from the presence of vegetation or, in the absence of leaves, due to high Froude numbers. The mean bed level, which corresponds to $z = 0$ m, was determined by identifying the z-coordinate of a line where the areas above and below the bed profile intersecting that line were equal in magnitude. The average water depth H was estimated as the average difference between the water surface elevation and the mean bed level.

The observed averaged bed and energy slopes, reported in Table 1, show a general agreement, suggesting the achievement of quasi-uniform flow conditions. The average bed slopes S_b from the 12●● and 1●●● setups exhibit a slight deviation of approximately 0.10% from the energy slope S_E. However, this deviation is considered negligible in the context of the study, since the presence of dunes in the flow field introduces local non-uniformity impacting the flow dynamics across the entire water depth, thus leading to minor discrepancies between the measured bed slope and energy slope. The uncertainty δ associated with the slopes was estimated using the 95%confidence interval of the linear fit parameters. On average, the uncertainty was found to be 0.009% for the bed slope and 0.002% for the energy slope (Table 1). Notably, setups with higher Froude numbers, that are generally associated with water surface effects (Naqshband et al., 2014), exhibited larger surface waves, leading to a more pronounced impact on the water surface elevation. The impact of surface and bed waves on slope determination was evaluated using the root mean square error (RMSE) of the linear regression (see Text S2 in Supporting Information S1). The average RMSE was found to be 0.16% for the bottom slope and reduced to 0.04% for the energy slope (Table 1). The RMSE related to the energy slope observed in the bare bed setup (0.08%) was eight times higher than that observed in the 1234 setup (0.01%).

The scanned bed profiles were also used to estimate the bedforms characteristics. However, for this analysis, only the topography data between $x = 12$m and $x = 21$m were considered to exclude the channel sections influenced by the inlet and outlet conditions. The wavelengths (λ_{crest}) were estimated using the zero-crossing technique by Van der Mark and Blom (2007). The zero-crossing technique involves removing the average bed slope from the bed elevation profiles and considering only bedforms that crossed the mean bed level. The wavelength of each bedform, denoted as λ_{crest}, was determined as the distance between consecutive crests. The average dune height (Δ_σ) was estimated using an empirical formulation proposed by Coleman et al. (2011) that establishes a relationship between the dune height and the standard deviation (σ) of the bed elevation profile, represented by $\Delta_\sigma = 2.2\sigma$, where the coefficient 2.2 was empirically derived using laboratory data and field measurements. The methodology by Lisimenka and Kubicki (2017) for determining dune wavelength and height was applied to validate the dune dimensions obtained from the equation derived by Coleman et al. (2011), Δ_σ, and from the zero-crossing method, λ_{crest}. This methodology utilizes spectral moments of the bed elevation profiles to evaluate dune heights and characteristic dune lengths. In this case, wavenumbers larger than 0.2 m^{-1} (corresponding to wavelengths larger than 5 m) were disregarded in order to focus on relevant dune characteristics. Further details regarding the formulations applied in this study are available in the Text S6 in Supporting Information S1.

Dune celerity was determined using footage from a side-view camera that recorded the lateral evolution of the bed elevation during each experimental run (Figure 2). The recording durations, which ranged from 45 to 90 min, were longer than the average dune migration period through the field of view, which varied from 4.5 to 12 min, with longer durations observed in setups with leafier vegetation. Each video tracked a minimum of five complete dunes. In each video frame, two different sections were selected, and a Matlab script (R2019b) was used to extract the relative bed elevation profiles. The celerity of the dunes was estimated by determining the time lag between the two bed evolution profiles, which was identified as the first positive peak of the cross-correlation function at a lag greater than zero. The dune celerity could then be estimated with the known distance between the two sections. All the side-view videos recorded during the experiments are available at the repository (Artini, 2024), offering insights into the dynamics of the experiments.

Furthermore, the measured sediment transport rates were compared to the outcomes of the sediment mass conservation principle in order to validate the celerity measurements. Commonly, in alluvial bed channels, the bed-load transport rate can be related to a volumetric sediment flux resulting from the movement of bedforms (Aberle et al., 2012; Cilli et al., 2021; Simons et al., 1965):

$$Q_{s,dune} = \beta \rho_s (1-p) c \Delta \qquad \left[m^2/s\right] \tag{1}$$

Here, $\beta = 0.5$ represents the coefficient factor associated with the assumption of a triangular dune shape, ρ_s is the sediment density and $p = 0.4$ is the porosity of the sand bed. The variables c and Δ represent the dune celerity and height, respectively.

The measured bed-load transport rates were compared to predicted values using classical sediment transport models based on bed shear stress proposed by van Rijn (1984a) and Einstein (1950)-Brown (1950). In applying these formulations, only parameters related to grain stress were considered to estimate the bed shear stress, as sediment transport is primarily influenced by skin friction (van Rijn, 1984a). Specifically, the grain-related friction velocity u'_* was estimated using the formula proposed by Engelund (1966), which has been recognized as effective in the presence of dunes (Van der Mark, 2009). The Engelund (1966) formulation consists in an iterative procedure to derive the value of u'_* (see Text S5 in Supporting Information S1). The values of u'_* were validated by determining the flow regime using the bedform stability diagram by Van den Berg and van Gelder (1993) and the flow regime classification by Brownlie (1983) (Figures S4–S5 in Supporting Information S1). These observations provided evidence supporting the reliability of the estimated skin friction values, along with the results regarding the prediction of the bed-load transport rates. Additionally, the measured bed-load transport rates were compared with predictions made by using the Armanini and Cavedon (2019) and Duan and Al-Asadi (2022) formulations which were developed for vegetated channels. Both studies simulated the presence of vegetation with rigid cylinders and observed mainly the formation of scour holes around the cylinder stems. All the formulations considered in this study are reported in the Text S6 in Supporting Information S1.

According to Maddux et al. (2003), unlike 2D dunes, the bed shear stress in the presence of 3D dunes cannot be predicted solely based on the spatially averaged Reynolds stress. Dunes with three-dimensional geometry were found to exhibit significantly higher resistance compared to 2D counterparts and this increased resistance was attributed to form-induced stress, associated to the presence of secondary currents. Applying the double-averaging methodology (Nikora et al., 2007) and assuming that the momentum balance close to the dune crest is governed by the turbulent and form induced stress (Maddux et al., 2003; McLean et al., 2008), the bed shear stress can be expressed as follows:

$$\tau_b = -\rho(\langle \overline{uw} \rangle + \langle \tilde{u}\tilde{w} \rangle) \tag{2}$$

where u and w represent velocity fluctuations in the longitudinal and vertical directions, respectively. The symbol $\sim$ denotes spatial variation, while the brackets $\langle\rangle$ indicate spatial averaging, and the overbar signifies temporal averaging. The predicted skin friction values, obtained from the formulation proposed by Engelund (1966) were then compared with the near-bed peak values of the fluid stress calculated using Equation 2.

Generally, in this study, the uncertainty related to estimates or measurements is calculated using the error propagation law (Text S2 in Supporting Information S1).

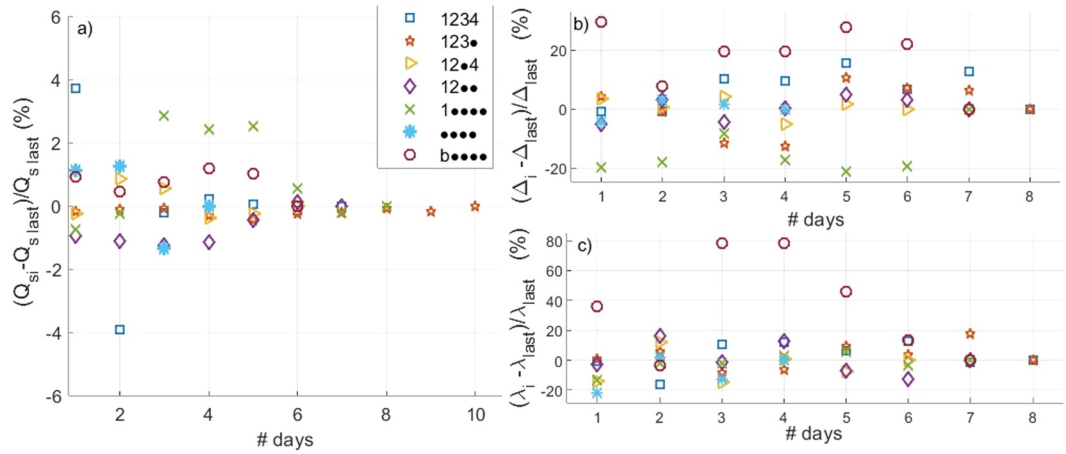

Figure 3. Percentage deviation between the daily and the last-day measurement for (a) sediment transport; (b) dune height and (c) dune wavelength. Each day represents 8 hr. For the 123• setup, the bed scans from the first two days were excluded due to technical issues.

3. Results

Each experimental setup was characterized by a different flow discharge due to the different foliage configuration. The variation in discharge was necessary to attain the desired hydraulic conditions, specifically to ensure the same just-submerged condition on the selected channel slope in all the setups. The reduction in channel conveyance, ΔQ reported in Table 1, indicates that the discharge for the leafiest setup was approximately 60% lower than that of the bare bed setup. This reduction in discharge clearly demonstrates the influential role of vegetation on flow characteristics, particularly its impact on channel conveyance. A similar reduction was documented by Aberle et al. (2011), who employed the same plants under comparable hydraulic conditions, but in a fixed plane bed setup.

To assess if the experiments were conducted under similar just-submerged conditions for the different experimental runs, the relative submergence of the plants was calculated as the ratio of the water depth (H) to the deflected plant height (h_p) at the highest point of the blossom, both measured at the same vertical (Figure S1 in Supporting Information S1). The resulting values for all the setups fell within the range of $1.13 < H/h_p < 1.16$ (Table S3 in Supporting Information S1). Since the water depth was consistent for all runs, it can be deduced that the degree of bending did not vary drastically among the experimental runs.

3.1. Morphological Equilibrium

The analysis of the temporal evolution of the percentage deviation between the daily-averaged sediment transport measurements Q_s and the value obtained from the final measurement provides insight into the attainment of morphological equilibrium. Figure 3a shows a fluctuating trend in the percentage variation over time, with a maximum value of 3–4%, mainly concentrated in the initial days. The percentage variation of dune characteristics over time follows a similar trend as the sediment transport, with deviations ranging between ±20% from the final measurement (Figures 3b and 3c). The b•••• setup showed a maximum deviation of up to 30% for dune height and significant deviation of ≈ 80% for the wavelength. However, these temporal discrepancies did not imply the unreliability of the collected measurements, as this setup was characterized by a high Froude number indicating a transition toward the upper regime, as confirmed by visual observations and subsequent analyses concerning the dune characteristics (Section 3.2). Therefore, higher variability in sediment transport and dune characteristics can be expected. For the subsequent analyses, the average values of measurements taken over the last 4 days of the experimental runs were considered to represent the morphological equilibrium state. This approach mitigates the influence of daily variations and provides a more reliable estimate of the overall characteristics of the sediment transport processes.

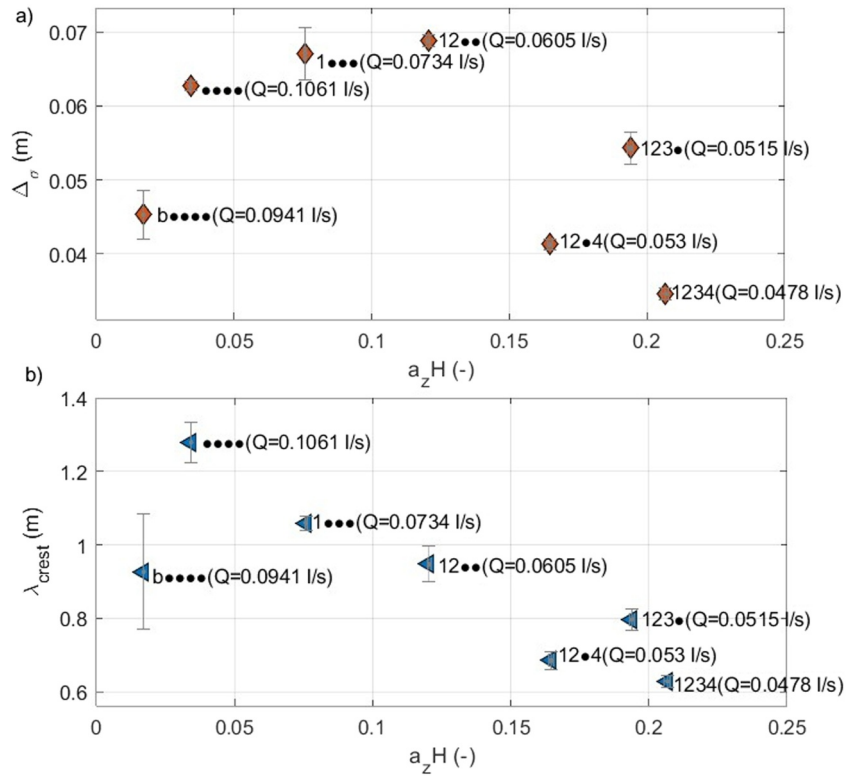

Figure 4. Measured average dune height Δ_σ (panel a) and dune wavelength λ_{crest} (panel b) plotted against the average frontal area per unit volume a_zH.

3.2. Dune Wavelength and Height

The bedforms exhibited varying characteristics across the setups in response to the diverse hydraulic conditions associated with the foliation stages. All observed bedforms were classified as dunes since the average wavelength exceeded 0.6 *m* (Perillo et al., 2014; Zanke & Roland, 2021) and agreed within the uncertainty levels with the outcomes of the formulations proposed by van Rijn (1984b) for predicting bedform geometry based on hydraulic parameters (Figure S6 in Supporting Information S1).

Figure 4 shows the relationship between dune geometry and roughness density, defined as the product of the average frontal area per unit volume of the plants and the water depth a_zH. The LAI is not used in this graph to include the setup without leaves. Furthermore, as a_zH decreases and thus flow discharge increases among the different setups, the dune height (Δ_σ) initially experienced a rapid growth, followed by a subsequent decay. This decay became more pronounced from setups with higher flow discharges, such as the 1••• setup and subsequent ones (Figure 4a and Table 2). These observations suggest a transition toward the upper flow regime, starting from the 1••• setup. The decay or washing out of the dunes, observed during these runs, can be associated with the erosion of dune crests, which is facilitated by higher suspended load (Naqshband et al., 2017) and Froude number exceeding 0.37 (Table 1). According to Naqshband et al. (2014), Froude numbers within the range of 0.32–0.84 are associated with significant free surface undulations that strongly influence bed morphology. Consequently, these free surface undulations lead to a rapid reduction in dune height as suspended transport increases. In this case, setups with higher flow discharges, such as the 1••• setup and subsequent ones, present a Froude number higher than 0.32 and decreasing trend for the dune height, thus confirming this observation (Figure 4a). Moreover, it is possible to observe the occurrence of mixed transport (bed-load and suspended) at high Froude numbers flows in the videos taken during the experiments and provided at the repository (Artini, 2024). On the other hand, the average dune wavelength increases with an increase in the water discharge, coinciding with a decrease in the average frontal area per unit volume of the plants (Figure 4b and Table 2).

Table 2
Estimated Dunes Characteristics

Setup	$\Delta_\sigma \pm S.E$ (cm)	$\Delta_{psd} \pm S.E.$ ($e(\Delta)$)(cm)	$\lambda_{crest} \pm S.E.$ (cm)	$\lambda_{psd} \pm S.E.$ ($e(\lambda)$)(cm)
1234	3.46 ± 0.087	3.56 ± 0.14 (2.9%)	62.82 ± 1.59	69.42 ± 1.02 (10.5%)
123•	5.43 ± 0.21	5.68 ± 0.21 (4.6%)	79.71 ± 2.94	82.88 ± 5.10 (4.0%))
12•4	4.13 ± 0.074	4.24 ± 0.05 (2.7%)	68.50 ± 2.49	78.00 ± 4.50 (13.9%)
12••	6.88 ± 0.077	7.06 ± 0.08 (2.6%)	94.74 ± 4.82	103.62 ± 2.29 (9.4%)
1•••	6.71 ± 0.36	6.94 ± 0.30 (3.4%)	105.93 ± 1.99	111.68 ± 1.97 (5.4%)
b••••	6.27 ± 0.069	6.24 ± 0.072 (−0.5%)	127.96 ± 5.47	148.99 ± 3.21 (16.4%)
••••	4.53 ± 0.32	4.60 ± 0.36 (1.5%)	92.66 ± 15.76	112.18 ± 16.16 (21.1%)

Note. The subscript *psd* indicate the outcomes of the Lisimenka and Kubicki (2017) model. $e(\Delta)$ and $e(\lambda)$ are the percentage errors between the *psd* values and the results obtained from the zero-crossing analysis (λ_{crest}) and the Coleman et al. (2011) Δ_σ. The standard error S.E.= SD/$\sqrt{n}$ with n numbers of measurements.

Table 2 and Figure 5 show the comparison between the values of λ_{crest} and Δ_σ and the results according to the spectral method proposed by Lisimenka and Kubicki (2017), denoted with the subscript "*psd*." The percentage deviation between the "*psd*" estimates and the values of λ_{crest} and Δ_σ was calculated using the following equation:

$$e(\lambda) = \frac{\lambda_{psd} - \lambda_{crest}}{\lambda_{crest}}; e(\Delta) = \frac{\Delta_{psd} - \Delta_\sigma}{\Delta_\sigma} \quad (3)$$

The Lisimenka and Kubicki (2017) method resulted in similar estimates of average dune heights and wavelengths, thereby confirming the initial estimates. However, the average percentage error between the two wavelength

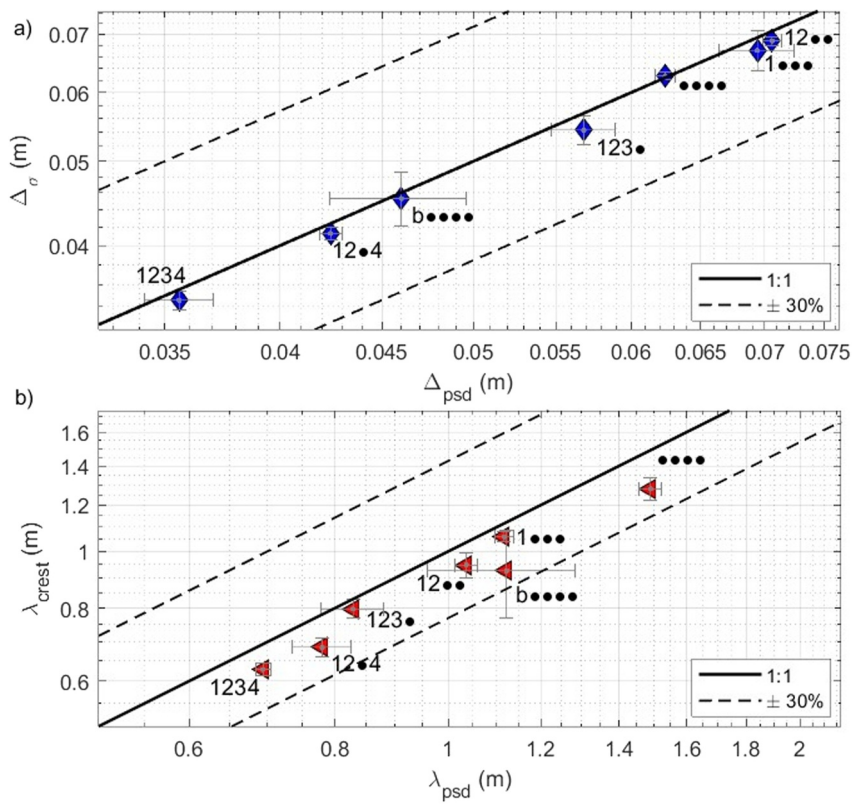

Figure 5. Comparison between the average dune characteristics obtained using Coleman et al. (2011) equation for Δ_σ, the zero-crossing method (Van der Mark & Blom, 2007) for λ_{crest} and Lisimenka and Kubicki (2017) equations for λ_{psd} and Δ_{psd}: (a) dune heights; (b) dune wavelength. The error bars represent the standard error of the estimated values.

Table 3
Measured Dune Celerity c_m and Sediment Transport Rate $Q_{s,m}$

Setup	c_m ± S.E. (m/s)	$\tau'_*(-)$	$Q_{s,m}$ (C($Q_{s,m}$)) (g/s)	$Q_{s,dune}(\pm e(Q_s))$ (g/s)
1234	8.45E−04 ± 3.18E−05	0.082 ± 0.0004	19.3 (0.5127)	13.9 ± 1.0 (−28%)
123•	8.25E−04 ± 1.08E−04	0.088 ± 0.0006	23.1 (0.5321)	23.8 ± 4.9 (3%)
12•4	9.19E−04 ± 7.48E−05	0.090 ± 0.0005	20.0 (0.6047)	16.3 ± 2.5 (−19%)
12••	1.19E−03 ± 2.07E−04	0.114 ± 0.0010	32.9 (0.5585)	39.1 ± 11.3 (19%)
1•••	1.75E−03 ± 5.00E−05	0.146 ± 0.0012	52.2 (0.5656)	56.0 ± 5.6 (7%)
b••••	3.25E−03 ± 5.00E−05	0.200 ± 0.0015	82.0 (0.5792)	97.2 ± 3.1 (19%)
••••	3.10E−03 ± 1.50E−03	0.244 ± 0.0016	87.1 (0.5196)	67.0 ± 54.6 (−23%)

Note. c_m is an average values of the videos recorded during the experiments, the standard error S.E.= SD/$\sqrt{n}$ with n numbers of measurements; $Q_{s,dune}$ is the estimate obtained using Simons et al. (1965) formula. e is the percentage difference between the $Q_{s,dune}$ and Q_s. $C = \sigma/\mu$ is the coefficient of variation of the Q_s measurements.

estimates was higher compared to that for the dune heights, specifically 15.7% compared to 1.6%. This deviation may be attributed to the differences in the employed methods, since the method proposed by Lisimenka and Kubicki (2017) relates the characteristic length of the dune to the peak of the spatial spectra, which could be influenced by the presence of secondary bedforms or vegetation, such as in the present case.

3.3. Dune Celerity and Sediment Transport

The celerities estimated from the side-view videos, reported in Table 3, were compared to predictions made using two different formulations available in the literature in order to evaluate their accuracy. The used formulations were the empirical relationship proposed by Tang and Knight (2006), which expresses celerity as a function of hydraulic conditions (water depth H and Froude number Fr) and the relationship proposed by Heydari et al. (2014) based on dimensional analysis. It is important to note that the Tang and Knight (2006) formulation was developed based on experimental data characterized by sediment sizes ranging from 0.18 to 2.28 mm, slope values in the range of 0.015% to 1.15% and Froude numbers between 0.2 and 0.8. We note also that the Heydari et al. (2014) formulation specifically takes into account sediment with a size of 0.85 mm and Froude numbers ranging from 0.24 to 0.73. The experimental data from the present study fall within the ranges covered by all the aforementioned works. The resulting comparison, illustrated in Figure 6 and reported in Table S7 in Supporting Information S1, reveals that the formulation proposed by Heydari et al. (2014) generally does not demonstrate strong correlation with the observed celerity. Moreover, the formulation proposed by Tang and Knight (2006) consistently underestimates the celerity in setups characterized by leafy vegetation. On the contrary, leafless setups exhibit reduced deviations from the agreement line. This disparity implies that the validity of this method might be compromised when leafy vegetation is present (see Table S7 in Supporting Information S1). This observation is consistent with the outcomes observed in bed-load bed-shear-stress based models predictions (see Section 4.1). Notably, the •••• setup shows a relatively better agreement among the other vegetated setups, suggesting a minimal influence of bare stems on dune celerity.

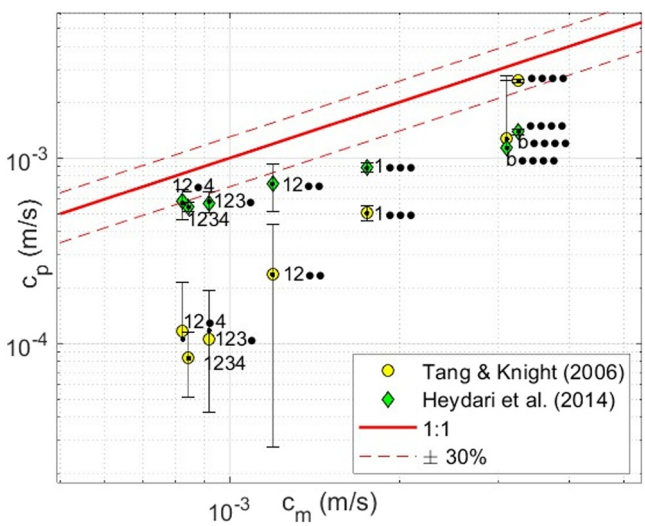

Figure 6. Dunes celerity estimates: comparison between measured and predicted values using Tang and Knight (2006) and Heydari et al. (2014).

The bed-load measurements clearly showed a sinuous trend of the instantaneous sediment transport rate corresponding to the succession of dunes entering the sediment-drain funnel (Figure S3 in Supporting Information S1). To analyze the time-dependent variability of the bed-load measurements, the coefficient of variation $C = \sigma/\mu$, where σ is the standard deviation and μ is the mean of the measured bed-load time series, was calculated for each experimental setup. The mean of the measurements from different days was considered for each setup, with the standard error across days for each setup ranging between 0.003 and 0.010. In Figure S7 in Supporting Information S1,

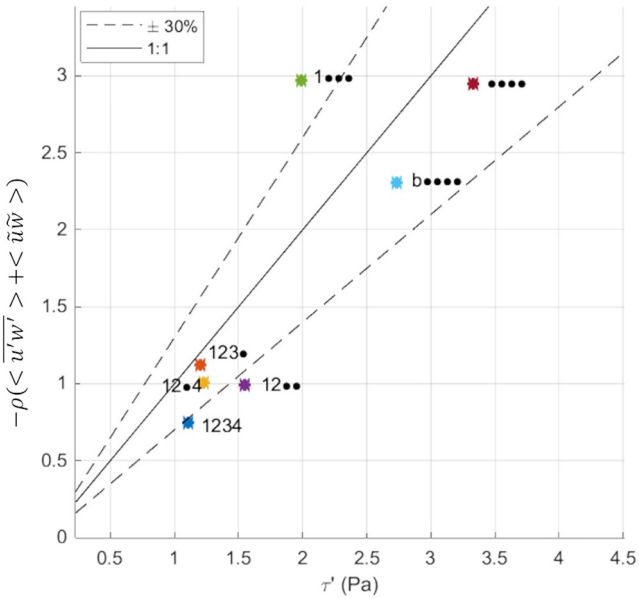

Figure 7. Comparison between the predicted skin friction τ' values and the peaks of the fluid shear stress inferred from the velocity measurements.

C is plotted against the flow discharge Q. Generally, C showed an increasing trend as the flow discharge Q increases for the majority of the setups. The data could be fitted with an exponential expression, yielding a coefficient of determination $R^2 = 0.88$, excluding the 12●4 and ●●●● setups. However, the differences in C values among the setups are not substantial, with C ranging from 0.513 to 0.605 (Table 3).

The skin friction values predicted using the proposed by Engelund (1966) formulation were compared with the near-bed peak values of fluid stress, calculated by summing Reynolds stresses and dispersive stress (Equation 2) to account for the local nonuniformity of flow over dunes (Maddux et al., 2003). As shown in Figure 7, the near-bed fluid stress peaks closely matched the skin friction values, exhibiting an average deviation of less than 30%, which validates the predicted skin friction values. Further validation of the derived u'_* values can be found in the Text S5 in Supporting Information S1.

The dune celerity values inferred from the side-view videos were employed to calculate $Q_{s,dune}$ using Equation 1. The results of the comparison between $Q_{s,dune}$ and the measured transport rates $Q_{s,m}$ are reported in Table 3 and Figure S8 in Supporting Information S1, along with the percentage error $e(Q_s)$ between the measured and computed values derived from the sediment mass conservation principle (Simons et al., 1965). The correlation between $Q_{s,dune}$ and $Q_{s,m}$ supports the validity of the celerity values inferred from the videos. The mean percentage error is approximately 20%, implying that the approach seems to be valid for approximating bed-load rates based solely on dune geometry, even in the presence of three-dimensional dunes. The average dune height estimated through longitudinal scans resulted a reliable indicator of dune geometry, even when dealing with three-dimensional dunes (details in Section 4.2).

4. Discussion

The following discussion addresses the effects of leafy vegetation on sediment transport and dune characteristics. To achieve this, the measured values were compared to the outcomes of available formulations, which were originally developed without considering vegetation and are thus taken to represent non-vegetated conditions. By comparing the predicted and measured quantities including sediment transport and dune characteristics, the influence of vegetation on these variables can be inferred.

4.1. Impact of Leafy Vegetation on Sediment Transport

The comparison between the predicted and measured sediment transport rates is summarized in Table S7 in Supporting Information S1 and Figure 8a. The Einstein-Brown (Brown, 1950; Einstein, 1950) and van Rijn (1984a) models provided predictions within ±≈ 30% deviation from the actual sediment transport rates for setups with low vegetation frontal area configurations (i.e., 1●●● and lower frontal area). However, for the bare stem setup (●●●● setup), the deviation between the predicted $Q_{s,p}$ and measured $Q_{s,m}$ bed load exceeded 30%. This could be due to the intensified suspended load observed during this experimental runs, characterized by higher Froude number, and thus, the potential limitations in capturing sediments by the recirculating system drain might have contributed to this deviation. Generally, for all the considered models, the deviation from the agreement line increased as the vegetation frontal area increased, reaching up to +80% for setup with the highest leaf mass (1234 setup). This suggests that the presence of leafy vegetation introduces additional complexities in sediment transport processes not accounted for by the considered bed-shear-stress-based models. Particularly, we observed that the presence of leaves near the bed promotes sediment resuspension (see Movie S1). This observation suggests that leaf movement contributes to sediment resuspension and may potentially enhance suspended sediment transport.

Moreover, the measured sediment transport rates were compared to predictions made using the Duan and Al-Asadi (2022) and Armanini and Cavedon (2019) bed-load models for vegetated channels. Particularly, Duan and

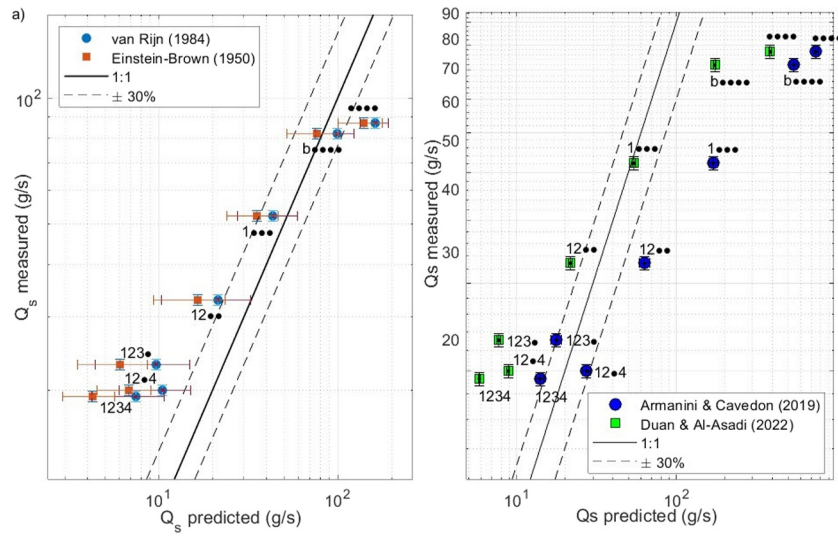

Figure 8. Sediment transport rates: (a) comparison between measured and predicted values using van Rijn (1984a) and Einstein-Brown (Brown, 1950; Einstein, 1950) models; (b) comparison between measured and predicted values using Armanini and Cavedon (2019) and Duan and Al-Asadi (2022) models. The black lines are the agreement line and those corresponding to a ± 30% deviation.

Al-Asadi (2022) method accounts for the areal density of the plants, while the Armanini and Cavedon (2019) formulation considered both the mean diameter (equivalent diameter in this case) and the areal vegetation density (Text S6 in Supporting Information S1). The comparison is shown in Figure 8b and Table Table S7 in Supporting Information S1. The Armanini and Cavedon (2019) method predicted sediment transport rates for the three leafiest setups with deviations ranging from 30% to 37%. Whereas, for the setups with lower frontal areas, the deviation increases as the plants frontal area reduces, with predicted bed-load rates being up to eight times higher. A similar trend was observed for the Duan and Al-Asadi (2022) predictions, although they generally underestimated sediment transport by a factor of 1.5–2, resulting in deviations of up to 70% for the leafiest setups. When applying the Armanini and Cavedon (2019) model considering a diameter value of 3 mm, which corresponds to the near-bed diameter for the 12●● setup and setups with lower frontal areas (i.e., characterized by bare stem near the bed), the predictions became unreliable, yielding non-physical values up to 1,000 g/s. Both models failed to predict sediment transport for setups characterized by lower frontal areas (leafless setups). This may be attributed to the fact that both models were originally developed under hydraulic conditions with Froude numbers less than 0.34 and in the absence of dunes.

These results suggest that the equivalent diameter of the vegetation, which correlates with the characteristic dimension of leaf-generated turbulence (Nepf, 2012), plays a significant role in enhancing sediment motion, being related to the sediment transport. Similar conclusions have been drawn in other studies (Tinoco & Coco, 2016; Yang & Nepf, 2018). The better agreement between the measured and predicted values with the Armanini and Cavedon (2019) model can be attributed to its consideration of the plant diameter in bed-load predictions. Furthermore, the enhancement in sediment transport seems to be more closely related to depth-averaged values rather than the near-bed roughness density of the vegetation.

According to Nepf (2012), in just-submerged conditions ($H \approx h_p$) the roughness density can be estimated as $a_z H$. For values in the range $0.1 < a_z H < 0.23$, conditions defined as "dense," the flow is characterized by canopy-scale turbulence over the entire water depth. For the present cases, $a_z H$ ranged from 0.2 to 0.02 (Table 4), and only 1●●●, b●●●● and ●●●● setups can be classified as sparse vegetation. Consequently, in all the other setups, a strong influence on the sediment processes can be expected from vegetation-related turbulence.

Indeed, the collected data show that the bed-load models based on bed shear stress seem to give acceptable results (i.e., within $\approx \pm 30\%$) for 1●●●, ●●●● and b●●●● setups, suggesting that it is possible to define a more precise validity threshold of these shear-stress-based models even in presence of vegetation. In particular, the roughness density $a_z H$ can be selected as threshold parameter and specifically $a_z H < 0.08$, that corresponds to the plant configuration with the upper branch only (1●●● setup). This suggests that the bed-shear-stress-based bed-load

Table 4
Frontal Area and Roughness Density

Setup	$A_f\ (cm^2)$	$\langle a \rangle_z\ (m^{-1})$	$a_z H(-)$	$A_{f,nb}\ (cm^2)$	$\langle a \rangle_{z,nb}\ (m^{-1})$	$a_{z,nb} H(-)$	$\lambda/H(-)$	$NDS \pm S.E(-)$
1234	72.0	0.933	0.207	4.98	0.250	0.055	2.84	1.32 ± 0.06
123•	67.0	0.863	0.194	1.99	0.099	0.022	3.55	1.12 ± 0.04
12•4	57.0	0.731	0.165	4.09	0.205	0.045	3.04	1.29 ± 0.07
12••	42.0	0.547	0.120	2.07	0.104	0.023	4.30	1.10 ± 0.02
1•••	27.0	0.341	0.076	2.13	0.106	0.024	4.77	1.09 ± 0.03
b••••	12.57	0.156	0.034	2.18	0.109	0.024	5.62	1.33 ± 0.07
••••	7.20	0.075	0.017	2.00	0.100	0.023	4.22	1.26 ± 0.02

Note. A_f is the plants frontal area. a_z is the depth-averaged frontal area per unit volume. $a_{z,nb} = mA_{f,nb}/H$ is the near-bed frontal area per unit volume related to the first 5 cm from the mean bed level. λ/H is the ratio between the average dune wavelength and the flow depth (Yalin, 1964). *NDS* is the non dimensional span (Venditti et al., 2005). The standard error S.E.= SD/$\sqrt{n}$ with n numbers of dunes observed in the considered DEM.

model remains valid in the presence of vegetation as long as the roughness density $a_z H$ is lower than 0.08. Moreover, the results emphasize that leafy vegetation has a notable impact on the flow field, leading to enhanced sediment transport for $a_z H > 0.08$. It is important to note that previous studies, commonly using rigid cylinders as a simplified representation of vegetation, reported a reduction in sediment transport with vegetation (Yager & Schmeeckle, 2013). However, the findings presented herein are specifically related to vegetation densities and characteristics used in the experimental activities.

4.2. Impact of Leafy Vegetation on Dune Geometry

To investigate the effect of the presence of leafy vegetation on dune geometry, the Yalin (1964) empirical relationship was tested using the experimental data collected during this study. Yalin (1964) claimed that dune wavelength scales with flow depth: $\lambda/H \approx 6-7$. The resulting ratios λ/H are reported in Table 4 for all the considered setups. It can be noted that λ/H decreases as the average plant frontal area, and thus areal density, increases, implying vegetation reduces dune length. Similarly, Penna et al. (2022) observed a reduction in bed undulation length with denser stem density. Particularly, the lowest λ/H values are related to the setups characterized by the lowest (near-bed) leaves.

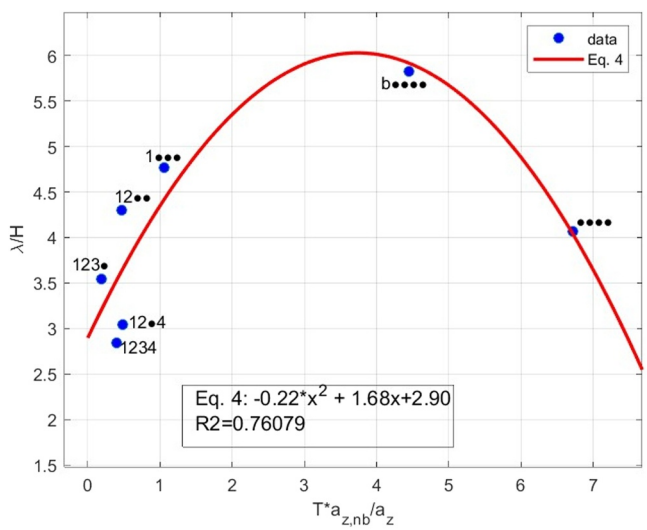

Figure 9. Equation 4, derived from curve fitting the experimental data, defines the relationship between λ/H and $T \cdot a_{z,nb}/a_z$.

To further investigate the relationship between the presence of near-bed leaves and the dune wavelength, the experimental data were plotted on a $\lambda/H - T \cdot a_{z,nb}/a_z$ plane, where $a_{z,nb}$ is the near-bed frontal area per unit volume, related to the first 5 cm from the bed and a_z is the depth-averaged frontal area per unit volume (Figure 9). The data were then curve-fitted, resulting in a parabolic equation, which reads:

$$\frac{\lambda}{H} = p_1\left(\frac{T \cdot a_{z,nb}}{a_z}\right)^2 + p_2\frac{T \cdot a_{z,nb}}{a_z} + p_3 \tag{4}$$

where T is the transport parameter (van Rijn, 1984a).

The fitted equation exhibits a high coefficient of determination ($R2 = 0.76$), and the resulting parameters along with their 95% confidence intervals are as follows:

- $p_1 = -0.2243 \quad (-0.4346, -0.01401)$
- $p_2 = 1.667 \quad (0.2622, 3.091)$
- $p_3 = 2.897 \quad (1.781, 4.012)$

A further analysis was conducted to explore the influence of vegetation on the three-dimensionality of dune geometry. This investigation involved the

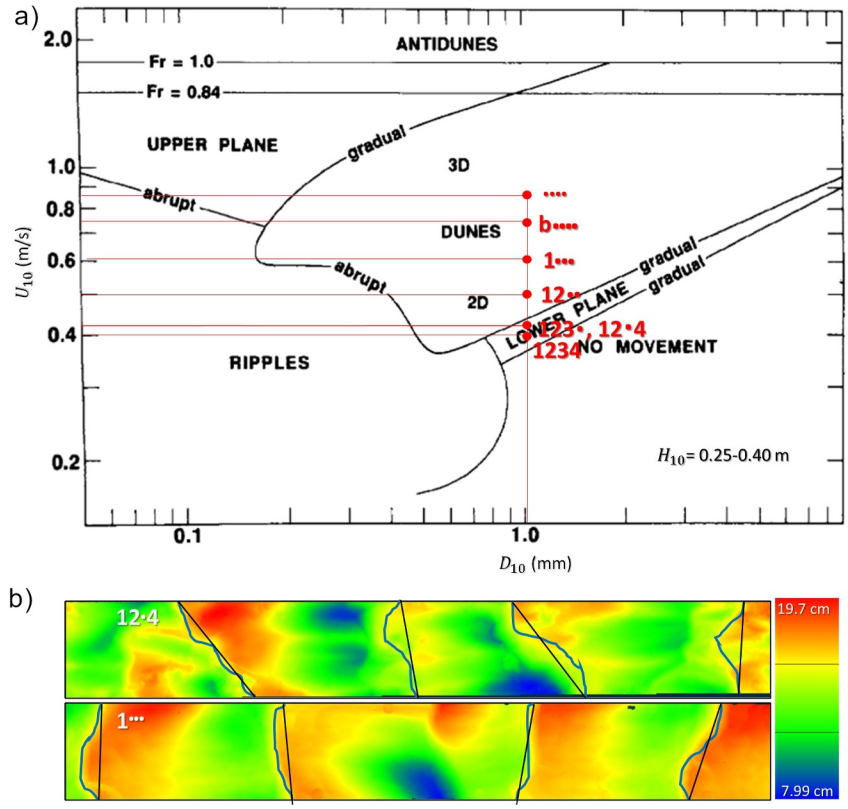

Figure 10. Dune geometry classification: (a) Southard and Boguchwal (1990) bedforms stability diagram, for H_{10} ranged between 0.25 and 0.40 m; (b) example of non-dimensional span estimation for 12•4 and 1••• setups on the basis of the built digital elevation model (Venditti et al., 2005). Figures S21–S26 in Supporting Information S1 show the DEMs of the other setups.

examination of available bedform stability diagrams to predict the 3D configuration of bedforms. A particular focus was set on the phase diagram by Southard and Boguchwal (1990) that delineates the hydraulic conditions under which three-dimensional (3D) dunes can form instead of two-dimensional (2D) dunes. The diagram accounts for temperature-standardized parameters such as depth d_{10}, flow velocity U_{10}, and sediment size D_{10} (Text S4 in Supporting Information S1). The results of this analysis are synthesized in Figure 10. Interestingly, the diagram predicts a three-dimensional geometry for setups with the lowest vegetation density, specifically the b•••• and •••• setups. In contrast, configurations characterized by the highest vegetation frontal area are classified as lower plane conditions. Notably, the corresponding section of the graph is labeled as "gradual," implying that the possibility of two-dimensional dunes cannot be entirely ruled out for these leafiest setups.

The assessment of bedform geometry classification, based on the Southard and Boguchwal (1990) diagram, was further compared with the classification proposed by Venditti et al. (2005), which refers to the non-dimensional span (NDS) or sinuosity of the dunes. NDS represents the ratio of the actual length of the crestline (depicted in blue in Figure 10b) to the straight-line distance between the endpoints of the crestline being analyzed (shown in black in Figure 10b). Values surpassing 1.2 indicate dunes with highly sinuous crestlines, a characteristic of three-dimensional bedforms (Venditti et al., 2005). To calculate NDS, the DEMs representing the final bed topography resulting from each experimental run were employed. Based on the NDS classification, only setups 123•, 12••, and 1••• were classified as two-dimensional, as detailed in Table 4. Particularly, setups initially predicted as 2D dunes according to the Southard and Boguchwal (1990) phase diagram, but characterized by the presence of the lowest branch, unexpectedly revealed a three-dimensional structure. This highlighted the considerable impact of the lowest branch on dune geometries, as the mobile dunes actively enveloped and covered the leaves of the lowest branch during their movement. In contrast, setups lacking the fourth branch exhibited agreement between the two classifications.

5. Conclusions

In conclusion, this work aimed to deepen the understanding of the intricate relationships between flow, sediment processes and vegetation, particularly focusing on the influence of vegetation on flow dynamics, sediment transport, and bedform development in fluvial environments. The findings of this study indicate that the presence of vegetation significantly affects dune geometry and therefore flow resistance. Notably, it is evident that the average dune wavelength tends to reduce as the plants frontal area increases. Furthermore, the bedform stability diagram by Southard and Boguchwal (1990) was found inaccurate in predicting the geometry of the observed bedforms when the lowest (near-bed) leaves are present and thus in direct contact with the bed sediments.

Indeed, the comparison between the measured bed-load transport rate and the outcomes of bed-shear-stress-based models, originally developed for bare bed conditions, showed that predictions within a $\approx 30\%$ percentage error are achievable for setups with lower vegetation roughness density, particularly with $a_z H < 0.08$. However, significant deviations occur for setups with vegetation characterized by higher frontal area, indicating the limitations of classical models in accurately predicting bed-load transport rate in such conditions. Particularly, the presence of the leafy vegetation seems to enhance sediments resuspension and facilitate bed-load transport. Moreover, the bed-load measurements were compared with predictions from models for flows with rigid cylinders. The model by Armanini and Cavedon (2019), which incorporates total shear velocity, grain size and vegetation parameters, such as mean diameter and areal density, aligns with the previous findings, albeit with around a 30% percentage error. Specifically, it confirms increased bed-load transport rates in vegetated channels compared to predictions from bed-shear-stress-based models for bare bed. On the contrary, the model by Duan and Al-Asadi (2022), which considers grain resistance and vegetation areal density, did not accurately predict bed-load transport rates for either the leafiest and leafless setups. The results highlight that the bed-load transport rate seems to be enhanced in the presence of leafiest plants, potentially due to the increased vegetation-generated turbulence, which scales with the characteristic diameter of the vegetation, a parameter considered in Armanini and Cavedon (2019). While Armanini and Cavedon (2019) formulation better predicted bed-load rates for the leafiest setups, substantial deviations were observed for setups with lower frontal areas. These findings suggest that when bedform drag is predominant over vegetation drag (e.g., in the case of leafless setups with $azH < 0.08$), the sediment transport is related to dunes dynamics. On the other hand, when the vegetation drag is higher (e.g., the same order of the bedforms drag), vegetation controls the sediment transport process.

It is noteworthy that the majority of previous studies on sediment transport in vegetated channels have relied on simplified vegetation models featuring rigid cylinders, thus overlooking the crucial interactions related to the presence of leaves and plant flexibility, that is, real-like vegetation. This study highlights the limitations of researches that relies on the simplification of rigid cylinders when modeling riparian vegetation. In this study, specifically, only the lowest branches were removed. It is worth considering further research to explore the consequences of removing leaves from the top while preserving those nearer to the bed. Additionally, conducting further studies under mobile-bed conditions and encompassing a wider range of leafy flexible vegetation densities, would be necessary to either validate or expand on the findings of this study. Such studies would be fundamental for enhancing the accuracy of models aimed at predicting the morphological evolution of natural river systems.

Data Availability Statement

Data concerning the characteristics of the plants are available through Jalonen et al. (2013) and Schoneboom (2011). The data set pertaining to the hydraulic conditions and measurements associated with flume experiments presented in this paper are openly available at the Zenodo repository (Artini, 2024). In the same repository, side-view videos recorded during the experiments are also included. The authors confirm that the data supporting the results and conclusions of this study are available within the article, its Supporting Information, and the repository.

Acknowledgments
This research fell within the framework of the SECURE project "Safety Equilibrium Conditions for rivers UndeR changing climatEs," funded by the European Union "Next Generation EU" (M4. C2.1.1).

References

Aberle, J., Coleman, S., & Nikora, V. (2012). Bed load transport by bed form migration. *Acta Geophysica*, *60*(6), 1720–1743. https://doi.org/10.2478/s11600-012-0076-y

Aberle, J., & Järvelä, J. (2013). Flow resistance of emergent rigid and flexible floodplain vegetation. *Journal of Hydraulic Research*, *51*(1), 33–45. https://doi.org/10.1080/00221686.2012.754795

Aberle, J., Schoneboom, T., & Rhiner, B. (2011). Influence of leaf mass on drag forces in vegetated flows. In *Proceedings of the 34th World Congress of the International Association for Hydro-environment Research and Engineering: Hydrology and Water Resources Symposium and Conference on Hydraulics in Water Engineering* (pp. 2744–2751).

Agisoft, L. (2017). Agisoft Photoscan Pro. Retrieved from https://www.agisoft.com

Antonarakis, A., Richards, K. S., Brasington, J., & Muller, E. (2010). Determining leaf area index and leafy tree roughness using terrestrial laser scanning. *Water Resources Research*, *46*(6). https://doi.org/10.1029/2009WR008318

Armanini, A., & Cavedon, V. (2019). Bed-load through emergent vegetation. *Advances in Water Resources*, *129*, 250–259. https://doi.org/10.1016/j.advwatres.2019.05.021

Artini, G. (2023). Linkages between flow, morphodynamics and vegetation (Doctoral dissertation, University of Florence). Retrieved from https://hdl.handle.net/2158/1350395

Artini, G. (2024). Effects of leafy flexible vegetation on bed-load transport and dune geometry [Dataset]. *Zenodo*. https://doi.org/10.5281/zenodo.11116395

Artini, G., Calvani, G., Francalanci, S., & Solari, L. (2021). Effects of vegetation at a bar confluence on river hydrodynamics: The case study of the Arno river at Greve junction. *River Research and Applications*, *37*(4), 615–626. https://doi.org/10.1002/rra.3774

Baas, J. H. (1994). A flume study on the development and equilibrium morphology of current ripples in very fine sand. *Sedimentology*, *41*(2), 185–209. https://doi.org/10.1111/j.1365-3091.1994.tb01400.x

Box, W., Järvelä, J., & Västilä, K. (2021). Flow resistance of floodplain vegetation mixtures for modelling river flows. *Journal of Hydrology*, *601*, 126593. https://doi.org/10.1016/j.jhydrol.2021.126593

Brown, C. B. (1950). Sediment transportation. *Engineering Hydraulics*, *12*, 769–857.

Brownlie, W. R. (1983). Flow depth in sand-bed channels. *Journal of Hydraulic Engineering*, *109*(7), 959–990. https://doi.org/10.1061/(ASCE)0733-9429(1983)109:7(959)

Cao, Z., Pender, G., & Meng, J. (2006). Explicit formulation of the shields diagram for incipient motion of sediment. *Journal of Hydraulic Engineering*, *132*(10), 1097–1099. https://doi.org/10.1061/(ASCE)0733-9429(2006)132:10(1097)

Chen, S.-C., Chan, H.-C., & Li, Y.-H. (2012). Observations on flow and local scour around submerged flexible vegetation. *Advances in Water Resources*, *43*, 28–37. https://doi.org/10.1016/j.advwatres.2012.03.017

Cilli, S., Billi, P., Schippa, L., Grottoli, E., & Ciavola, P. (2021). Bedload transport and dune bedforms characteristics in sand-bed rivers supplying a retreating beach of the northern Adriatic Sea (Italy). *Journal of Hydrology: Regional Studies*, *37*(6), 100894. https://doi.org/10.1016/j.ejrh.2021.100894

Cloud compare. (2022). Retrieved from https://www.cloudcompare.org

Coleman, S. E., Nikora, V. I., & Aberle, J. (2011). Interpretation of alluvial beds through bed-elevation distribution moments. *Water Resources Research*, *47*(11). https://doi.org/10.1029/2011WR010672

D'Ippolito, A., Calomino, F., Dey, S., Gaudio, R., & Penna, N. (2023). Bedload transport through emergent vegetation: Current status and its future prospect. *Environmental Fluid Mechanics*, *23*(3), 711–733. https://doi.org/10.1007/s10652-023-09918-0

Duan, J. G., & Al-Asadi, K. (2022). On bed form resistance and bed load transport in vegetated channels. *Water*, *14*(23), 3794. https://doi.org/10.3390/w14233794

Einstein, H. A. (1950). *The bed-load function for sediment transportation in open channel flows (No. 1026)*. US Department of Agriculture. https://doi.org/10.22004/ag.econ.156389

Engelund, F. (1966). Hydraulic resistance of alluvial streams. *Journal of the Hydraulics Division*, *92*(2), 315–326. https://doi.org/10.1061/JYCEAJ.0001417

Follett, E. M., & Nepf, H. M. (2012). Sediment patterns near a model patch of reedy emergent vegetation. *Geomorphology*, *179*, 141–151. https://doi.org/10.1016/j.geomorph.2012.08.006

Griffin, E. R., Perignon, M. C., Friedman, J. M., & Tucker, G. E. (2014). Effects of woody vegetation on overbank sand transport during a large flood, Rio Puerco, New Mexico. *Geomorphology*, *207*, 30–50. https://doi.org/10.1016/j.geomorph.2013.10.025

Gurnell, A. (2014). Plants as river system engineers. *Earth Surface Processes and Landforms*, *39*(1), 4–25. https://doi.org/10.1002/esp.3397

Heydari, H., Zarrati, A., & Karimaee Tabarestani, M. (2014). Bed form characteristics in a live bed alluvial channel. *Scientia Iranica*, *21*(6), 1773–1780.

Holloway, J. V., Rillig, M. C., & Gurnell, A. M. (2017). Physical environmental controls on riparian root profiles associated with black poplar (Populus nigra l.) along the Tagliamento River, Italy. *Earth Surface Processes and Landforms*, *42*(8), 1262–1273. https://doi.org/10.1002/esp.4076

Hongwu, T., Wang, H., Liang, D., Lv, S., & Yan, L. (2013). Incipient motion of sediment in the presence of emergent rigid vegetation. *Journal of Hydro-Environment Research*, *7*(3), 202–208. https://doi.org/10.1016/j.jher.2012.11.002

Huai, W.-x., Li, S., Katul, G. G., Liu, M.-y., & Yang, Z.-h. (2021). Flow dynamics and sediment transport in vegetated rivers: A review. *Journal of Hydrodynamics*, *33*(3), 400–420. https://doi.org/10.1007/s42241-021-0043-7

Jalonen, J., Järvelä, J., & Aberle, J. (2013). Leaf area index as vegetation density measure for hydraulic analyses [Dataset]. *Journal of Hydraulic Engineering*, *139*(5), 461–469. https://doi.org/10.1061/(ASCE)HY.1943-7900.0000700

Järvelä, J. (2004). Determination of flow resistance caused by non-submerged woody vegetation. *International Journal of River Basin Management*, *2*(1), 61–70. https://doi.org/10.1080/15715124.2004.9635222

Le Bouteiller, C., & Venditti, J. (2015). Sediment transport and shear stress partitioning in a vegetated flow. *Water Resources Research*, *51*(4), 2901–2922. https://doi.org/10.1002/2014WR015825

Lei, J., & Nepf, H. (2021). Evolution of flow velocity from the leading edge of 2-d and 3-d submerged canopies. *Journal of Fluid Mechanics*, *916*, A36. https://doi.org/10.1017/jfm.2021.197

Lisimenka, A., & Kubicki, A. (2017). Estimation of dimensions and orientation of multiple riverine dune generations using spectral moments. *Geo-Marine Letters*, *37*(1), 59–74. https://doi.org/10.1007/s00367-016-0475-1

Lokin, L., Warmink, J., Bomers, A., & Hulscher, S. (2022). River dune dynamics during low flows. *Geophysical Research Letters*, *49*(8), e2021GL097127. https://doi.org/10.1029/2021GL097127

Luhar, M., & Nepf, H. M. (2013). From the blade scale to the reach scale: A characterization of aquatic vegetative drag. *Advances in Water Resources*, *51*, 305–316. https://doi.org/10.1016/j.advwatres.2012.02.002

Maddux, T., McLean, S., & Nelson, J. (2003). Turbulent flow over three-dimensional dunes: 2. Fluid and bed stresses. *Journal of Geophysical Research*, *108*(F1), 6010. https://doi.org/10.1029/2003JF000017

McLean, S., Nikora, V., & Coleman, S. (2008). Double-averaged velocity profiles over fixed dune shapes. *Acta Geophysica*, *56*(3), 669–697. https://doi.org/10.2478/s11600-008-0031-0

Meyer-Peter, E., & Müller, R. (1948). Formulas for bed-load transport. In *Proceedings of the 2nd meeting of the International Association for Hydraulic Structures Research* (pp. 39–64).
Morgan, J. A., Brogan, D. J., & Nelson, P. A. (2017). Application of structure-from-motion photogrammetry in laboratory flumes. *Geomorphology*, *276*, 125–143. https://doi.org/10.1016/j.geomorph.2016.10.021
Naqshband, S., Hoitink, A., McElroy, B., Hurther, D., & Hulscher, S. J. (2017). A sharp view on river dune transition to upper stage plane bed. *Geophysical Research Letters*, *44*(22), 11437–11444. https://doi.org/10.1002/2017GL075906
Naqshband, S., Ribberink, J. S., & Hulscher, S. J. (2014). Using both free surface effect and sediment transport mode parameters in defining the morphology of river dunes and their evolution to upper stage plane beds. *Journal of Hydraulic Engineering*, *140*(6). https://doi.org/10.1061/(ASCE)HY.1943-7900.0000873
Nepf, H. M. (2012). Hydrodynamics of vegetated channels. *Journal of Hydraulic Research*, *50*(3), 262–279. https://doi.org/10.1080/00221686.2012.696559
Nikora, V., McEwan, I., McLean, S., Coleman, S., Pokrajac, D., & Walters, R. (2007). Double-averaging concept for rough-bed open-channel and overland flows: Theoretical background. *Journal of Hydraulic Engineering*, *133*(8), 873–883. https://doi.org/10.1061/(ASCE)0733-9429(2007)133:8(873)
Palmer, M. A., Bernhardt, E., Allan, J., Lake, P. S., Alexander, G., Brooks, S., et al. (2005). Standards for ecologically successful river restoration. *Journal of Applied Ecology*, *42*(2), 208–217. https://doi.org/10.1111/j.1365-2664.2005.01004.x
Parker, G. (2003). Persistence of sediment lumps in approach to equilibrium in sediment-recirculating flumes. In *XXX International Association of Hydraulic Research Congress, Thessaloniki, Greece*.
Penna, N., Coscarella, F., D'Ippolito, A., & Gaudio, R. (2022). Effects of fluvial instability on the bed morphology in vegetated channels. *Environmental Fluid Mechanics*, *22*(2), 619–644. https://doi.org/10.1007/s10652-022-09832-x
Perillo, M. M., Best, J. L., Yokokawa, M., Sekiguchi, T., Takagawa, T., & Garcia, M. H. (2014). A unified model for bedform development and equilibrium under unidirectional, oscillatory and combined-flows. *Sedimentology*, *61*(7), 2063–2085. https://doi.org/10.1111/sed.12129
Przyborowski, Ł., Łoboda, A. M., & Bialik, R. J. (2018). Experimental investigations of interactions between sand wave movements, flow structure, and individual aquatic plants in natural rivers: A case study of Potamogeton Pectinatus l. *Water*, *10*(9), 1166. https://doi.org/10.3390/w10091166
R2019b. (2019). *Matlab version: 9.13.0 (r2019b)*. The MathWorks Inc. Retrieved from https://www.mathworks.com
Richardson, D. M., Holmes, P. M., Esler, K. J., Galatowitsch, S. M., Stromberg, J. C., Kirkman, S. P., et al. (2007). Riparian vegetation: Degradation, alien plant invasions, and restoration prospects. *Diversity and Distributions*, *13*(1), 126–139. https://doi.org/10.1111/j.1366-9516.2006.00314.x
Rowiński, P. M., Västilä, K., Aberle, J., Järvelä, J., & Kalinowska, M. B. (2018). How vegetation can aid in coping with river management challenges: A brief review. *Ecohydrology and Hydrobiology*, *18*(4), 345–354. https://doi.org/10.1016/j.ecohyd.2018.07.003
Schoneboom, T. (2011). Widerstand flexibler vegetation und sohlenwiderstand in durchströmten bewuchsfeldern (Resistance of flexible vegetation and sole resistance in flow through vegetation fields) [Dataset]. *Dissertation, Braunschweig, Technische Universität Braunschweig*. https://doi.org/10.24355/dbbs.084-201112141024-0
Schoneboom, T., & Aberle, J. (2009). Influence of foliage on drag force of flexible vegetation. In *33rd IAHR Congress* (pp. 9–14).
Schoneboom, T., Aberle, J., Wilson, C. A., & Dittrich, A. (2008). Drag force measurements of vegetation elements. In *ICHE 2008. Proceedings of the 8th International Conference on Hydro-science and Engineering, September 9-12, 2008*.
Simons, D. B., & Richardson, E. V. (1966). Resistance to flow in alluvial channels. In *Chapter. Geological survey professional paper (422-J)*. US Government Printing Office. https://doi.org/10.3133/pp422J
Simons, D. B., Richardson, E. V., & Nordin, C. F. (1965). Bedload equation for ripples and dunes. In *Chapter. Geological survey professional paper (462-H)*. US Government Printing Office. https://doi.org/10.3133/pp462H
Southard, J. B., & Boguchwal, L. A. (1990). Bed configuration in steady unidirectional water flows; Part 2, Synthesis of flume data. *Journal of Sedimentary Research*, *60*(5), 658–679. https://doi.org/10.1306/212f9241-2b24-11d7-8648000102c1865d
Tang, X., & Knight, D. W. (2006). Sediment transport in river models with overbank flows. *Journal of Hydraulic Engineering*, *132*(1), 77–86. https://doi.org/10.1061/(ASCE)0733-9429(2006)132:1(77)
Tinoco, R. O., & Coco, G. (2016). A laboratory study on sediment resuspension within arrays of rigid cylinders. *Advances in Water Resources*, *92*, 1–9. https://doi.org/10.1016/j.advwatres.2016.04.003
Van den Berg, J., & van Gelder, A. (1993). A new bedform stability diagram, with emphasis on the transition of ripples to plane bed in flows over fine sand and silt. *Spec. Publs. Int. Ass.Sediment*, *17*, 11–21. https://doi.org/10.1002/9781444303995.ch2
Van der Mark, C. (2009). A semi-analytical form drag model for river bedforms (Doctoral dissertation, University of Twente, Enschede, Netherlands). https://doi.org/10.3990/1.9789036528665
Van der Mark, C., & Blom, A. (2007). A new and widely applicable tool for determining the geometric properties of bedforms. *Civil Eng. & Man. Res. Reports 2007R-003/WEM-002*. https://doi.org/10.13140/RG.2.2.17637.40161
van Dijk, W. M. (2013). *Meandering rivers-feedbacks between channel dynamics, floodplain and vegetation* (Doctoral dissertation) Utrecht University. https://www.researchgate.net/publication/237150878_Meandering_rivers_-_feedbacks_between_channel_dynamics_floodplain_and_vegetation
van Rijn, L. C. (1984a). Sediment transport, Part I: Bed load transport. *Journal of Hydraulic Engineering*, *110*(10), 1431–1456. https://doi.org/10.1061/(ASCE)0733-9429(1984)110:10(1431)
van Rijn, L. C. (1984b). Sediment transport, Part III: Bed forms and alluvial roughness. *Journal of Hydraulic Engineering*, *110*(12), 1733–1754. https://doi.org/10.1061/(ASCE)0733-9429(1984)110:12(1733)
Vargas-Luna, A., Crosato, A., & Uijttewaal, W. S. (2015). Effects of vegetation on flow and sediment transport: Comparative analyses and validation of predicting models. *Earth Surface Processes and Landforms*, *40*(2), 157–176. https://doi.org/10.1002/esp.3633
Venditti, J. G., Church, M., & Bennett, S. J. (2005). On the transition between 2d and 3d dunes. *Sedimentology*, *52*(6), 1343–1359. https://doi.org/10.1111/j.1365-3091.2005.00748.x
Wang, X., Gualtieri, C., & Huai, W. (2023). Grain shear stress and bed-load transport in open channel flow with emergent vegetation. *Journal of Hydrology*, *618*, 129204. https://doi.org/10.1016/j.jhydrol.2023.129204
Xu, Y., & Nepf, H. (2020). Measured and predicted turbulent kinetic energy in flow through emergent vegetation with real plant morphology. *Water Resources Research*, *56*(12). https://doi.org/10.1029/2020WR027892
Yager, E., & Schmeeckle, M. (2013). The influence of vegetation on turbulence and bed load transport. *Journal of Geophysical Research: Earth Surface*, *118*(3), 1585–1601. https://doi.org/10.1002/jgrf.20085
Yalin, M. S. (1964). Geometrical properties of sand wave. *Journal of the Hydraulics Division*, *90*(5), 105–119. https://doi.org/10.1061/JYCEAJ.0001097

Yang, J. Q., Chung, H., & Nepf, H. (2016). The onset of sediment transport in vegetated channels predicted by turbulent kinetic energy. *Geophysical Research Letters*, *43*(21), 11261–11268. https://doi.org/10.1002/2016GL071092

Yang, J. Q., & Nepf, H. M. (2018). A turbulence-based bed-load transport model for bare and vegetated channels. *Geophysical Research Letters*, *45*(19), 10428–10436. https://doi.org/10.1029/2018GL079319

Yang, J. Q., & Nepf, H. M. (2019). Impact of vegetation on bed load transport rate and bedform characteristics. *Water Resources Research*, *55*(7), 6109–6124. https://doi.org/10.1029/2018WR024404

Zanke, U., & Roland, A. (2021). On ripples—A boundary layer-theoretical definition. *Water*, *13*(7), 892. https://doi.org/10.3390/w13070892

Zinke, P. (2012). Application of porous media approach for vegetation flow resistance. In *Proceedings of River Flow 2012 San Jose (Costa Rica) 5-7 September* (pp. 301–310).

References From the Supporting Information

Coles, D. (1956). The law of the wake in the turbulent boundary layer. *Journal of Fluid Mechanics*, *1*(2), 191–226. https://doi.org/10.1017/S0022112056000135

Dietrich, W. E. (1982). Settling velocity of natural particles. *Water Resources Research*, *18*(6), 1615–1626. https://doi.org/10.1029/WR018i006p01615

Muste, M., Lyn, D. A., Admiraal, D., Ettema, R., Nikora, V., & García, M. H. (2017). *Experimental hydraulics: Methods, instrumentation, data processing and management: Volume I: Fundamentals and methods*. CRC Press.

Popiel, C., & Wojtkowiak, J. (1998). Simple formulas for thermophysical properties of liquid water for heat transfer calculations (from 0 C to 150 C). *Heat Transfer Engineering*, *19*(3), 87–101. https://doi.org/10.1080/01457639808939929

Zonta, F., Marchioli, C., & Soldati, A. (2012). Modulation of turbulence in forced convection by temperature-dependent viscosity. *Journal of Fluid Mechanics*, *697*, 150–174. https://doi.org/10.1017/jfm.2012.67